Journal of Theoretical and Applied Mechanics, Sofia, Vol.55 (2025) pp. 52-62
SPECIAL ISSUE

INFLUENCE OF THE ASPECT RATIO ON THE THERMAL STRATIFICATION IN UNDERGROUND SENSIBLE THERMAL ENERGY STORAGE

M. RASHEVSKI*

Institute of Mechanics, Bulgarian Academy of Sciences

[Received: 6 January 2025. Accepted: 12 March 2025]

doi: https://doi.org/10.55787/jtams.25.55.1.052

ABSTRACT: Thermal stratification due to natural convection in underground long-term hot water storage is simulated numerically over 180 days. The mathematical model is based on the unsteady two-dimensional Navier-Stokes-Fourier equations with Boussinesq approximation. Dynamic temperature boundary conditions are applied on the cavern walls. Finite difference method (FDM) is used to solve the problem in vorticity-stream function formulation. Three different cavern aspect ratios are considered. The evolution of vortices and its influence on the temperature and velocity fields is presented through graphics at the end of the studied period. The thermocline thickness and the Nusselt numbers on the cavern walls are determined. The calculations show that the highest aspect ratio leads to better thermal stratification and thermally more efficient storage design.

KEY WORDS: Unsteady natural convection, Incompressible viscous fluid, Numerical simulation, Thermal stratification, Sensible thermal energy storage.

1 INTRODUCTION

Thermal energy storage (TES) is a crucial technology in the energy transition of this century and its role is expected to increase in the near future [1, 2]. Its application stretches among various sectors, e.g. increasing grid capacities in the energy sector, utilization of waste heat, domestic hot water appliances, harvesting of renewable energies, increasing thermal mass and off-grid installations in the building sector, [3] etc. Although space is an important factor and some studies deal with latent [4] or thermochemical [5] storage systems with increased capacity per cubic meter, the sensible thermal energy storage (STES) remains the most reliable and cheap way to accumulate energy in the long run [6].

Different STES designs have been used and continuous research aims at optimization and accurate prediction of storage performance. The energy densities in such systems are studied and compared by numerous authors. For example in [7, 8] it is shown that the highest practical usability of the common materials in terms of

*Corresponding author e-mail: mrashevski@imbm.bas.bg

cost, volume and reliability possesses the hot water storage, which is often buried underground to save space. In their critical review Dahash et al. [9] indicate again the water as the most practically available material for STES. The authors discuss the geometry of the buried TES in regard to the external thermal losses due to compactness of the storage (A/V ratio) and internal exergetic losses arising due to decay of stratification in the storage depending on its aspect ratio (AR). The two most common geometries are the vertical hot water tank and the shallow pit storage, the latter one usually with considerably larger volumes. While the external losses play less role in well insulated tank, the internal exergetic losses are considerable and should be evaluated accordingly. That is why the aspect ratio is important topic of investigation by many previous experimental [10–12], theoretical [13–17] works. In [13–15] the researchers conclude that an AR of 4 is the most beneficial for the proper storage stratification, while Hariharan et al. [10], Nelson et al. [16] and Al-Kandari et al. [11] suggest AR values between 3 and 4. The authors agree that further increase of the aspect ratio has negligible effect. Nevertheless, quadratic, or close to quadratic designs should be considered as well, because they benefit from better A/V ratio and less external losses.

The present work builds on author's previous research [18] and considers the cooling of a closed rectangular two-dimensional domain with time-dependent temperature boundary conditions. Natural convection and heat transfer for three different aspect ratios are simulated numerically over 6 months using FDM. The influence of the AR on the thermal losses, velocity field and thermal stratification of the storage at the end of the studied period is discussed.

2 Formulation of the problem

The thermal energy storage is modeled by a closed symmetric rectangular tank with plane walls of width d and height H. Starting from an initial still state with a uniform temperature T_{init}, the storage medium (water) begins motion and cools down over a period of 180 days due to convection thermal losses through the four walls. Three different aspect ratios are studied $AR = \frac{H}{d} = 4$ (Case 1), $AR = 1$ (Case 2) and $AR = \frac{1}{4}$ (Case 3), but with the same relative internal area (Fig. 1). The convection in the cavern is assumed laminar and is described by the unsteady incompressible Navier-Stokes-Fourier equations with the Boussinesq approximation. The governing equations are expressed in their vorticity-stream function form [18, 19]:

$$\frac{\partial \omega}{\partial t} + \frac{\partial \psi}{\partial y}\frac{\partial \omega}{\partial x} - \frac{\partial \psi}{\partial x}\frac{\partial \omega}{\partial y} = Pr\nabla^2\omega + RaPr\frac{\partial T}{\partial x}\,, \tag{1}$$

$$\frac{\partial T}{\partial t} + \frac{\partial \psi}{\partial y}\frac{\partial T}{\partial x} - \frac{\partial \psi}{\partial x}\frac{\partial T}{\partial y} = \nabla^2 T\,, \tag{2}$$

$$-\omega = \frac{\partial^2 \psi}{\partial x^2} + \frac{\partial^2 \psi}{\partial y^2}\,, \tag{3}$$

$$u = \frac{\partial \psi}{\partial y},\ \ v = -\frac{\partial \psi}{\partial x},\ \ \omega = -\frac{\partial u}{\partial y} + \frac{\partial v}{\partial x}\,, \tag{4}$$

where u and v are x and y velocity components, ψ stream function, ω vorticity, ν kinematic viscosity, $\kappa = k/(\rho C_p)$ thermal diffusivity, k thermal conductivity, C_P specific heat capacity, β thermal expansion coefficient and T dimensionless temperature. The scales used are d, κ/d, ρ, d^2/κ and $\Delta T = T_{\text{init}} – T_{\text{inf}}$ for length, velocity, density, time and temperature, respectively. The dimensionless parameters involved are the Prandtl number $Pr = \nu/\kappa$ and the Rayleigh number $Ra = g\beta d^3 \Delta T/(\kappa\nu)$. If $\tilde{H} = H/d$ is the dimensionless height of the cavern, the non-slip boundary and initial conditions for system (1-3) can be written as:

$$\frac{\partial \psi}{\partial x} = \frac{\partial \psi}{\partial y} = 0 \quad \text{at } x = 0:1, y = 0 \text{ and } y = \tilde{H} \text{ for } t > 0, \tag{5}$$

$$\frac{\partial \psi}{\partial x} = \frac{\partial \psi}{\partial y} = 0 \quad \text{at } y = 0:\tilde{H}, x = 0 \text{ and } x = 1 \text{ for } t > 0, \tag{6}$$

$$\psi = \omega = 0 \text{ at } x = 0:1, y = 0:\tilde{H} \text{ for } t = 0, \tag{7}$$

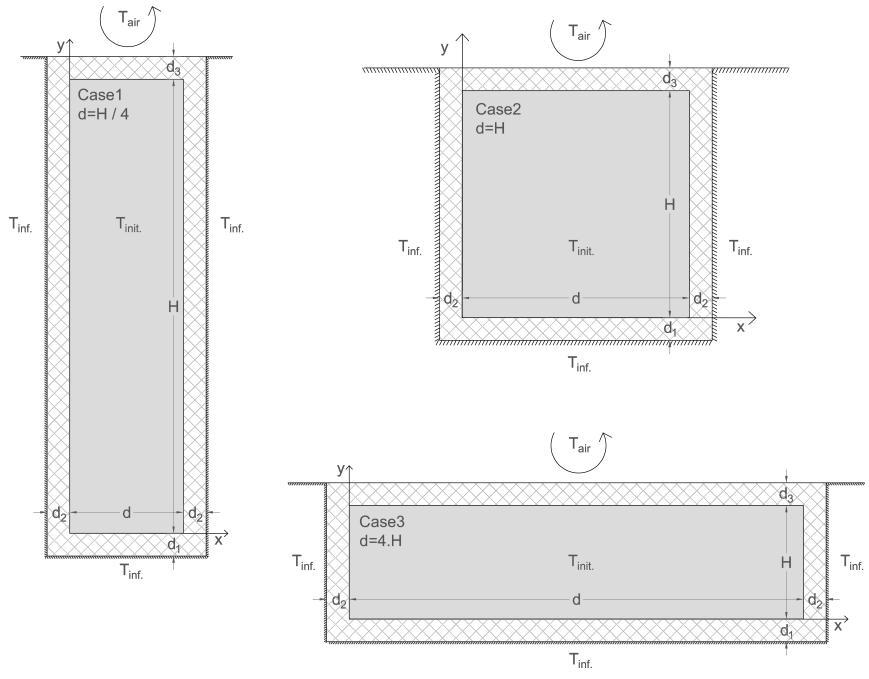

Fig. 1. Geometry of the underground hot water storage at the initial state t=0 for the three cases under consideration.

The temperature boundary conditions model the heat transfer through the storage walls with three different insulation thicknesses. They change over the studied period of time in a way described in details in [18]. System (1-3) with the corresponding boundary conditions is solved by finite difference method using an explicit scheme.

3 RESULTS

In the following section some results for the streamlines, velocity and temperature are presented in dimensional form for three cavern geometries of the studied aspect ratios H/d (m/m): 20/5, 10/10 and 5/20. The numerical simulations are executed for $T_{\text{init}} = 363.15$ K (90°C), $T_{\text{inf}} = 288.15$ K (15°C), $T_{\text{air}} = 273.15$ K (0°C), and the corresponding thermal properties of water at 363 K: $\nu = 3.35 \times 10^{-7}$ [m^2/s], $\kappa = 1.66 \times 10^{-7}$ [m^2/s], $C_P = 4207$ [J/(kgK)], $k = 0.67$ [W/mK], $\beta = 7 \times 10^{-4}$ [K^{-1}]. The bottom boundary insulation thickness is $d_1 = 0.7$ m, the side walls have insulation thickness $d_2 = 0.8$ m, and the top wall: $d_3 = 1.2$ m. The thermal conductivity of the insulating material is $k_{\text{ins}} = 0.032$ [W/mK]. The calculations are executed for $Pr = 1.965$, which corresponds to the initial water temperature and

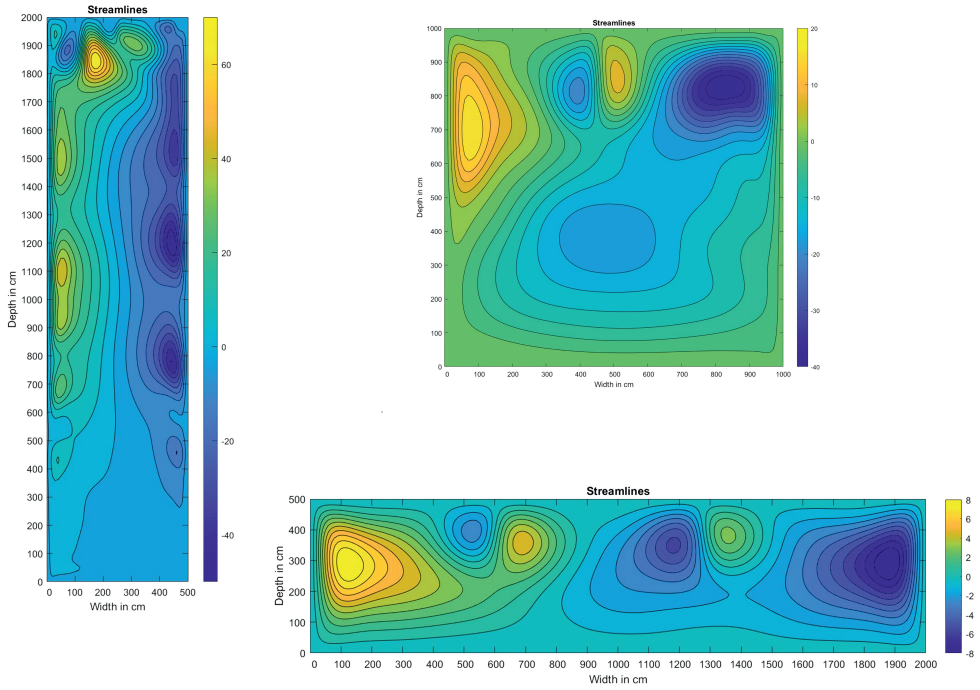

Fig. 2. Streamlines for cases 1 (left), 2 (right) and 3 (below).

for $Ra = 10^9$. The graphics are plotted at the final time step of the simulation period. Some important thermal characteristics such as the thermocline and the Nusselt number on the cavern walls are determined.

3.1 STREAMLINES

Figure 2 shows the results for the streamlines. The intensity and direction of the vortices are demonstrated through the colors of the graphics. The negative values of the stream function (blue) stay for a clockwise direction of the flow, while the positive values (yellow) – for a counter-clockwise. In all of the studied cases the vortices are mostly located close to the vertical and top walls. The greatest number of vortices is observed in the high narrow storage, but they affect a small part of the internal area. In the other two cases there are fewer vortices, but they entrain larger fluid areas, which leads to less thermal stratification in the storage.

3.2 VELOCITY FIELD

Figure 3 demonstrates the corresponding velocity fields observed in the three tanks. It is noteworthy to mention that in the shallow cavern thermal cellular convection is observed, similar to the Benard-Rayleigh cells.

Table 1 summarizes the numerical results for the velocity components U and V and the maximum of the velocity magnitude $W = \sqrt{(U^2 + V^2)}$. In all three cases $W_{\max}$ is close to the absolute value of the vertical velocity component $V_{\min}$ directed downwards. Hence, the absolute maximum velocity occurs close to the vertical side walls where the fluid slips down the cool boundaries and where hardly any transverse velocity is present ($U \approx 0$).

Table 1. Maximum and minimum of the velocity components U, V and $W_{\max}$ in cm/min

AR	$U_{\max}$	$V_{\max}$	$U_{\min}$	$V_{\min}$	$W_{\max}$
4:1	5.86	7.58	-7.13	-14.67	14.86
1:1	7.39	4.54	-4.68	-10.45	10.45
1:4	2.63	1.48	-2.68	-5.02	5.03

3.3 TEMPERATURE FIELD

Figure 4 shows the calculated temperature fields. The effect of the vortices in entraining storage medium, affects strongly the formation of clearly observable stratified areas.

The maximum, mean and minimum temperatures ($T_{\max}$, T_{mean} and $T_{\min}$ respectively) are given in Table 2. In the shallow cavern the temperature drop is the most

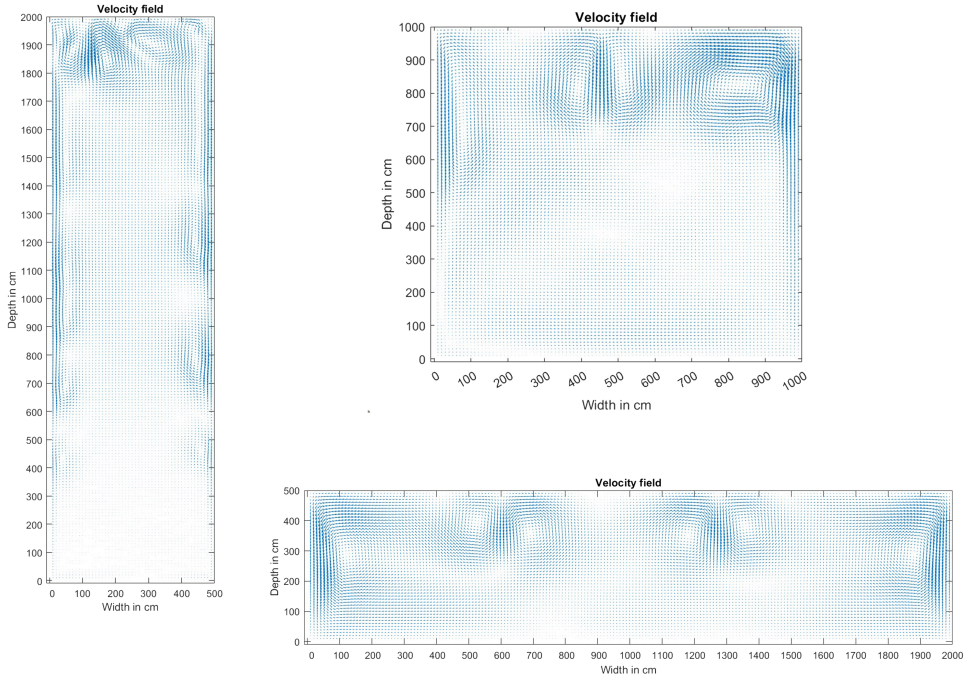

Fig. 3. Velocity fields for cases 1 (left), 2 (right) and 3 (below).

significant due to the higher convective thermal losses. On the other hand, the largest value of the temperature difference $\delta T = T_{\max} - T_{\min}$ is observed in the high narrow channel because of the stronger stratification and lower thermal losses. It is also the case where the mean temperature of the water is highest, hence, most useful thermal energy is stored over the studied period.

Table 2. Temperature values $T_{\max}$, T_{mean} and $T_{\min}$ in °C and maximum temperature difference δT for $Ra = 10^9$ after 180 days

AR	$T_{\max}$	T_{mean}	$T_{\min}$	δT
4:1	89.0550	88.5905	86.2348	2.8202
1:1	88.1547	87.7592	86.3369	1.8178
1:4	83.8175	83.6689	83.1559	0.6616

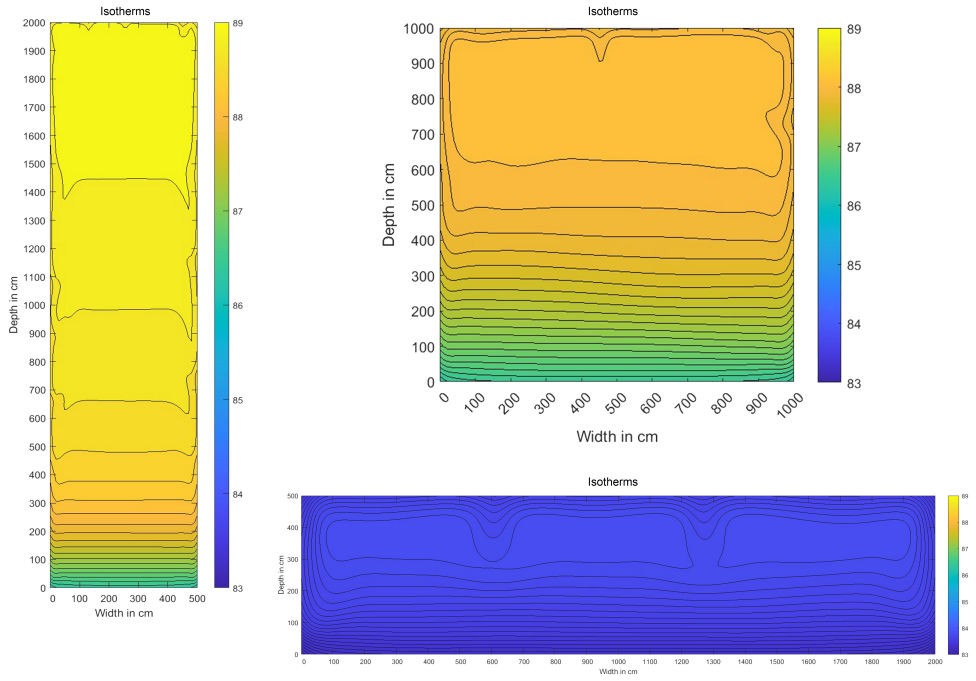

Fig. 4. Temperature fields for cases 1 (left), 2 (right) and 3 (below).

3.4 THERMAL CHARACTERISTICS

Two main thermal characteristics are studied - the formation of thermocline and the Nusselt number on the side, top and bottom walls.

Thermocline thickness:

The thermocline thickness is defined by the region of rapid temperature change [20]. There is no strict definition about which area it involves, but here it is assumed that the thermocline occurs in the area where the dimensionless temperature

$$\Theta = \frac{T - T_{\min}}{\delta T} \tag{8}$$

is less than 0.80. Figure 5 shows Θ in the middle section of the thermal storage after 180 days for the three aspect ratios under consideration. The case with strongest thermal stratification is the high narrow storage where the thermocline occurs in about 20% of the height of the cavern. In the rest of the reservoir there is a well separated (stratified) warm fluid area. In the quadratic geometry the thermocline is less

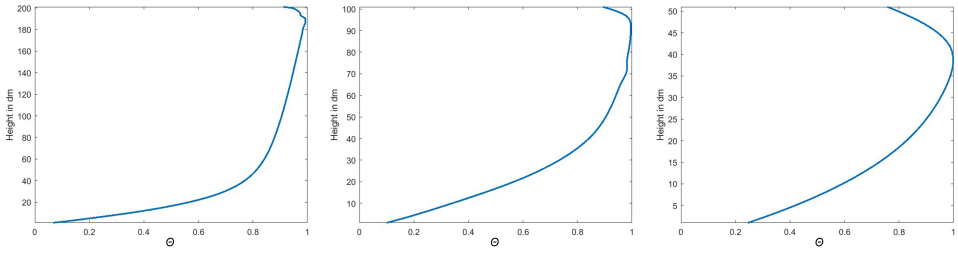

Fig. 5. Vertical profile of Θ in the middle section for $AR = 4, 1$ and 1/4 (from left to right).

pronounced and occupies about 30% of the storage height, while in the shallow reservoir there is hardly any thermocline observed and the temperature changes gradually throughout the whole fluid body. Note that the closed cavern has no cold water area in the bottom part, because there is no cold water inlet.

Nusselt number:

The average Nusselt number on the storage walls is defined as the ratio between the convective and conductive heat fluxes [18]:

$$\overline{Nu} = \frac{q_{\text{conv}}}{q_{\text{cond}}}\,, \tag{9}$$

where

$$q_{\text{conv}} = -\frac{k}{\tilde{H}} \int_0^{\tilde{H}} \frac{\partial T}{\partial x} dy\,,$$
$$q_{\text{cond}} = -\frac{k}{\tilde{H}} \int_0^{\tilde{H}} \frac{\partial T_{\text{cond}}}{\partial x} dy\,.$$

Figure 6 shows the variations of the Nusselt number for the time period of 180 days. In all three cases the highest Nusselt number is the one at the top wall, and the lowest Nusselt number is at the bottom wall, because of the different wall insulation thicknesses. There are periodic fluctuations observed in the values for the top and side walls, which are resulting from the periodic formation and disintegration of vortices in these areas of the cavern which contribute to higher convective losses and eventually affect the Nusselt number. In the shallow cavern there is less difference between the side walls and the bottom of the cavern. The linear decline of the Nusselt numbers with respect to the time period is due to the high mixing processes and the gradual cooling of the fluid body as a whole.

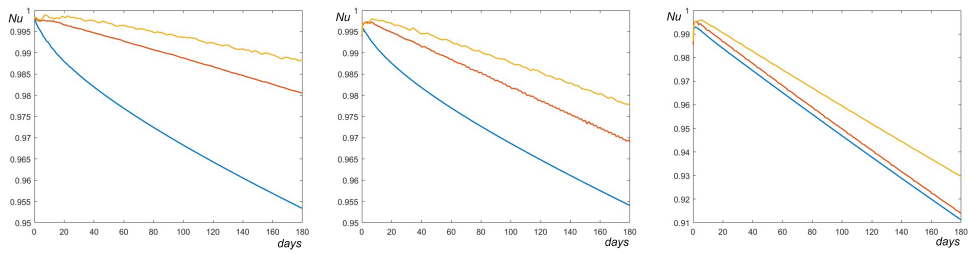

Fig. 6. Nusselt numbers on the bottom (blue), side (red) and top (yellow) walls of the thermal storage over 180 days. From left to right $AR = 4, 1$ and 1/4.

4 Conclusions

Unsteady natural convection in closed rectangular caverns, resembling underground sensible thermal energy storage, is modeled through the Navier-Stokes-Fourier with Boussinesq approximation. The effect of the aspect ratio on the velocity and the temperature fields is investigated through numerical simulations of three different geometries with the same enclosed area using water as a storage medium and starting from a still state with a uniform initial temperature.

Graphical and numerical results for the streamlines, velocity and temperature are obtained for $Ra = 10^9$ through an explicit FDM scheme. It is shown that the buoyant force accelerates the fluid along the vertical planes of the cavern, which naturally leads to a maximum velocity vector observed in the narrow vertical storage. It is also the case with the greatest number of vortices which are intensive, but affect small part of the internal area. In the other geometries under consideration there are fewer vortices, but they entrain larger fluid areas, which leads to a less prominent thermal stratification of the storage. The higher temperature difference and the higher mean temperature of the water in the narrow vertical storage indicates that this aspect ratio is theoretically more beneficial for accumulation of large amounts of thermal energy. Furthermore, the thermocline thickness and the Nusselt number are calculated. It is demonstrated that these thermal characteristics are strongly affected by the aspect ratio of the cavern and by the resulting convection patterns with periodic formation and disintegration of vortices. The thermocline thickness of the high narrow storage is clearly visible and occupies only about 20% of the storage height, while a well distinguished thermocline in the shallow cavern hardly exists.

Finally, the study shows that the higher aspect ratios lead to more efficient and better stratified thermal energy storage. The results from the simulation can help engineers or designers to compare the benefit from the storage efficiency with respect to the expected overcost for deeper excavation works. The mathematical model

gives truthful results with limited computational resources and may be used for other rectangular geometries with symmetric base.

ACKNOWLEDGEMENTS

This work was supported by the Bulgarian Ministry of Education and Science under the National Research Programme "Young scientists and postdoctoral students-2" approved by DCM 206/07.04.2022.

REFERENCES

[1] K.M. TAN, T.S. BABU, V.K. RAMACHANDARAMURTHY, P. KASINATHAN, S.G. SOLANKI, S.K. RAVEENDRAN'(1993) Empowering smart grid: A comprehensive review of energy storage technology and application with renewable energy integration. *Journal of Energy Storage* **39** 102591.

[2] S. CHAVAN, R. RUDRAPATI, S. MANICKAM (2022) A comprehensive review on current advances of thermal energy storage and its applications. *Alexandria Engineering Journal* **61** 5455–5463.

[3] M. RASHEVSKI, S. SLAVTCHEV (2023) Some problems related to the mathematical modeling of convection flows in water flow glazing. *Journal of Theoretical and Applied Mechanics* **53** 366-388.

[4] H. JOUHARA, A. ZABNIENSKA-GORA, N. KHORDEHGAH, D. AHMAD, T. LIPINSKI (2020) Latent thermal energy storage technologies and applications: A review. *International Journal of Thermofluids* **5-6** 100039.

[5] J. COT-GORES, A.F. CASTELL, L. CABEZA (2012) Thermochemical energy storage and conversion: A-state-of-the-art review of the experimental research under practical conditions. *Renewable and Sustainable Energy Reviews* **16** 5207-5224.

[6] A.V. NOVO, J.R. BAYON, D. CASTRO-FRESNO, J. RODRIGUEZ-HERNANDEZ (2010) Review of seasonal heat storage in large basins: Water tanks and gravel–water pits. *Applied Energy* **87** 390-397.

[7] T. SCHMIDT, D. MANGOL, A. MUELLER-STEINHAGEN (2003) Seasonal thermal energy storage in Germany. In: *ISES Solar World Congress*

[8] A.I. FERNANDEZ, M. MARTINEZ, M. SEGARRA, I. MARTORELL, L. CABEZA (2010) Selection of materials with potential in sensible thermal energy storage. *Solar Energy Materials Solar Cells* **94** 1723–1729.

[9] A. DAHASH, F. OXE, M. JANETTI (2019) Advances in seasonal thermal energy storage for solar district heating applications: A critical review on large-scale hot-water tank and pit thermal energy storage systems. *Applied Energy* **239** 296–315.

[10] K. HARIHARAN, K. BADRINARAYANA, S.S. MURTHY, M.V. MURTHY (1991) Temperature stratification in hot-water storage tanks. *Energy* **16** 977-982.

[11] A. AL-KANDARI, S. MOUSTAFA, A. AL-MARAFIE (2004) Effect of geometry on static thermal stratification. In: *Second Arab Int. Solar Energy Conf.*

[12] A.J.N. KHALIFA, A.T. MUSTAFA, F.A. KHAMMAS (2011) Experimental Study of Temperature Stratification in a Thermal Storage Tank in the Static Mode for Different Aspect Ratios. *Journal of Engineering and Applied Sciences* **6** 53-60.

[13] R.L. COLE, F.O. BELLINGER (1982) Thermally stratified tanks. *ASHRAE Transactions* **88** 1005-1017

[14] K.A.R. ISMAIL, J.F.B. LEAL, M.A. ZANARDI (1997) Models of Liquid Storage Tanks. *Energy* **22** 805-815.

[15] E. HAHNE, Y. CHEN (1998) Numerical study of flow and heat transfer characteristics in hot water stores. *Solar Energy* **64** 9-18.

[16] J.E.B. NELSON, A.R. BALAKRISHNAN, S.S. MURTHY (1999) Parametric studies on thermally stratified chilled water storage systems. *Applied Thermal Engineering* **19** 89-115.

[17] W. YAICI, M. GHORAB, E. ENTCHEV, S. HAYDEN (2013) Three-dimensional unsteady CFD simulations of a thermal storage tank performance for optimum design. *Applied Thermal Engineering* **60(1-2)** 152–163.

[18] M. RASHEVSKI, S. SLAVTCHEV (2024) Convective thermal losses of long-term underground hot water storage. *Journal of Thermal Engineering* **10(2)** 490–502.

[19] Y. JALURIA (1980) "Natural Convection. Heat and Mass Transfer". Pergamon Press, Oxford, UK, pp. 977-982.

[20] W. BAHNFLETH, A. MUSSER (1998) Thermal performance of a full-scale stratified chilled-water thermal storage tank. *ASHRAE Transactions* **104** 377–388.